International Journal of QUANTUM CHEMISTRY

Linear Augmented Cylindrical Wave Method for Nanotubes Electronic Structure

Pavel N. D'yachkov

In this review paper, the main ideas and results of application of the linearized augmented cylindrical wave (LACW) method for the electron properties of the single-walled, double-walled, embedded, and intercalated nanotubes are summarized. We start with the simplest case of the achiral single-walled (n, 0) and (n, n) tubules having small translational unit cells. Then, the electron properties of chiral (n, m) nanotubes having very large translational cells are discussed with account of tubules possessing rotational and screw symmetries. Based on the LACW and Green's function techniques, the *ab initio* numerical approach to calculating the electron local densities of states of the substitutional impurities in the nanotubes is presented. The relativistic version of LACW theory is described and applied to calculating the effects of spin–orbit coupling on π-bands of the cumulenic $(C)_n$ and polyynic $(C_2)_n$ carbynes and armchair tubules. The approach of the cylindrical waves applied for the description of nanotubes permits to reproduce their geometry in an explicit form that offers the great advantages. © 2015 Wiley Periodicals, Inc.

DOI: 10.1002/qua.25000

Introduction

Carbon nanotubes are the giant cage-like molecules looking like closed hollow cylindrical shells.[1] The electronic structure of all-carbon nanotubes have received much attention since 1992, when the first calculations on the electron band structures of the single-wall nanotubes were done in the terms of the Hückel type tight-binding technique.[2–5] Since 90s,[6,7] we are developing a linearized augmented cylindrical wave method (LACW) for the nanotubes band structure at our laboratory. The LACW method is an extension to the one-dimensional multiatomic systems with cylindrical or tubular structure of the augmented plane wave (APW) theory suggested by J. Slater in 1937 for the bulk materials and developed latter by O. K. Andersen, D. D. Koelling, and G. O. Arbman in a form of linearized APW (LAPW) technique.[8–11] In this review, we briefly outline the physical basis and some applications of the LACW technique. This method was emerged and developed in our laboratory; perhaps, this justifies an unusually large number of references to our publications in the bibliography.

The structure of this article is as follows. Initially, the necessary information on the nanotubes geometry is provided. A presentation of LACW method begins with a description of the method for constructing the muffin-tin electron potentials for the tubular and cylindrical polyatomic systems. The next section is devoted to the theoretical basis of the method on the examples of non-chiral single-walled nanotubes. Here, we present also the results of numerical calculations of couple of carbon nanotubes with armchair and zigzag geometries and the semiconducting and metallic types of electron band structures. Further, considering the screw and rotational symmetry of nanotubes, the methods of calculations of chiral systems based on the techniques of LACW and Green's functions are described. The latter are used also for calculating the electronic properties of point defects in the nanotubes, which are illustrated by examples of the density of electronic states in the vicinity of nitrogen and boron substitutional impurities. The next two sections are devoted, respectively, to investigations of the effects of the interlayer tunneling of electrons on the electronic characteristics of the double-walled nanotubes and to analysis of electronic properties of samples in the form of single-walled nanotubes embedded in a semiconductor matrix. Next, we discuss the nanorods in the form of nanotubes, the inner cavity of which is filled with transition metals. In the last part of this article, a brief summary of the relativistic version of the LACW method is given and spin-orbit gaps in metallic carbon nanotube and carbines are discussed.

Nanotubes' Structure

The single-walled nanotubes can be considered as a result of sewing of corresponding graphene nanoribbons.[12] The C—C bond length $d_{C-C} = 1.42$ Å and a pair of positive integers $n_1 \geq n_2$, determine the spatial arrangement of atoms in a three-dimensional structure of tubule. Figure 1 shows that, in the non-chiral single-walled (n, n) armchair and (n, 0) zigzag nanotubes, the two bonds of each hexagon are oriented perpendicular and parallel to the nanotube symmetry Z axis, respectively. Generally, the tubes are chiral with intermediate hexagons orientation with respect to Z axis. The translational cells of non-chiral tubes are relatively small, while they can be huge in the chiral tubes.

P. N. D'yachkov
Quantum Chemistry Laboratory, Kurnakov Institute of General and Inorganic Chemistry, Russian Academy of Sciences, Leninskii Pr. 31, Moscow 119991, Russian Federation
E-mail: p_dyachkov@rambler.ru

Contract grant sponsor: Russian Foundation for Basic Research; contract grant number: 14-03-00493.

Pavel N. D'yachkov was born in Saint Petersburg (the former Leningrad) in 02.12.1947. He was educated in Moscow and Leningrad State Universities, Chemistry Departments; graduated from Quantum Chemistry Chair founded by V. A. Fock. His interests are the quantum chemistry of nanomaterials and coordination compounds and modeling of the toxic and cancerogenic effects of environmental pollutants. Author of five books including "Heteroligand Molecules: Structure, Isomers, Transformations" (Francis and Taylor, London and New York, 2002, 271 p; with Alexander A. Levin).

Nanotubes Cylindrical Muffin-Tin Potential

The original both nonrelativistic[10,11] and relativistic[14–17] LAPW techniques for bulk materials are based on a muffin-tin (MT) approximations for electronic potentials. That is, the potential $V(\mathbf{r})$ is constructed to be the spherically symmetric in the regions of atoms and constant between them. Our method is based on the MT approach too.[6,7,18–20] However, there is a great difference between the bulk and nanomaterials, because an electron transport is unlimited in all directions in the first case, while in nanotubes it is surely determined by the size and tubular shape. Therefore, MT method must be slightly adapted to the cylindrical structures.

According to the cylindrical MT approximation, we consider the tube to be positioned between infinite barriers Ω_a and Ω_b, which separate the multiatomic system between the two vacuum regions Ω_v outside and inside of tubule (Fig. 2). The radii $a = R_{NT} + \delta$, $b = R_{NT} - \delta$ depend on a radius of tubule R_{NT} and a distance 2δ between Ω_a and Ω_b barriers. Practically, we use the $2\delta = 4.6$ a.u., which predicts the valence band width values equal to about 22 eV for all single-walled nanotubes. Similar to the APW/LAPW model, we also apply a $\rho^{1/3}$ local density exchange potential,[20] where the electron density $\rho(\mathbf{r})$ of tubule being calculated as a superposition of atomic densities. Inside the MT spheres, its spherically symmetric part $\rho(r)$ is taken. In the interspherical space, the potential $V(\mathbf{r}) = 0$ is taken as the energy zero point.

Single-Walled Armchair and Zigzag Nanotubes

Let us start from the simplest case of the achiral single-walled armchair and zigzag nanotubes.[6,7,17–24] Such tubules have relatively small cells, and the computer calculations can be performed with account of translational symmetry only. In our

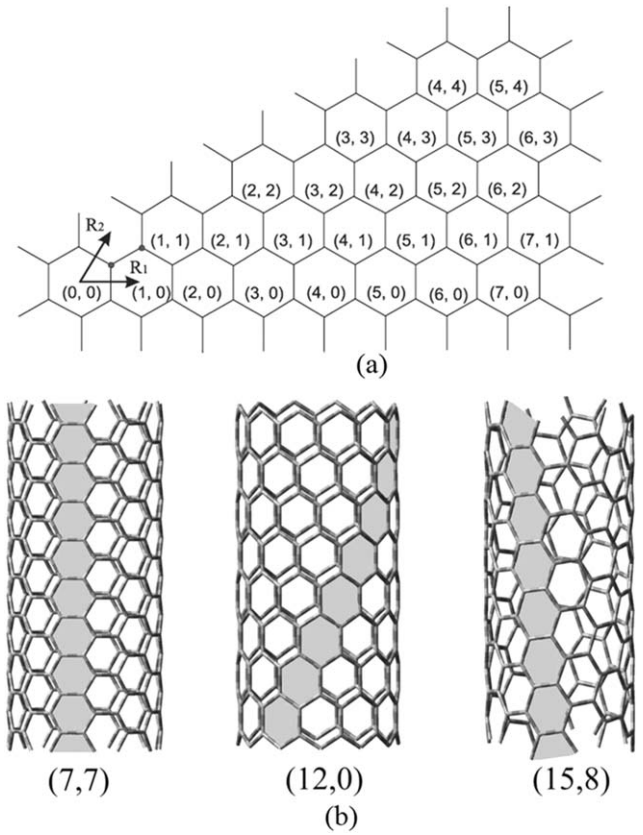

Figure 1. (a) Graphene monolayer with indexed lattice sites. Rolling the layer from (0,0) to ($n1$, $n2$) point gives a single-walled ($n1$, $n2$) tubule. (b) Examples of armchair (7,7), zigzag (12,0), and chiral (15,8) nanotubes. (Reproduced from Ref. 13, with permission from American Physical Society.).

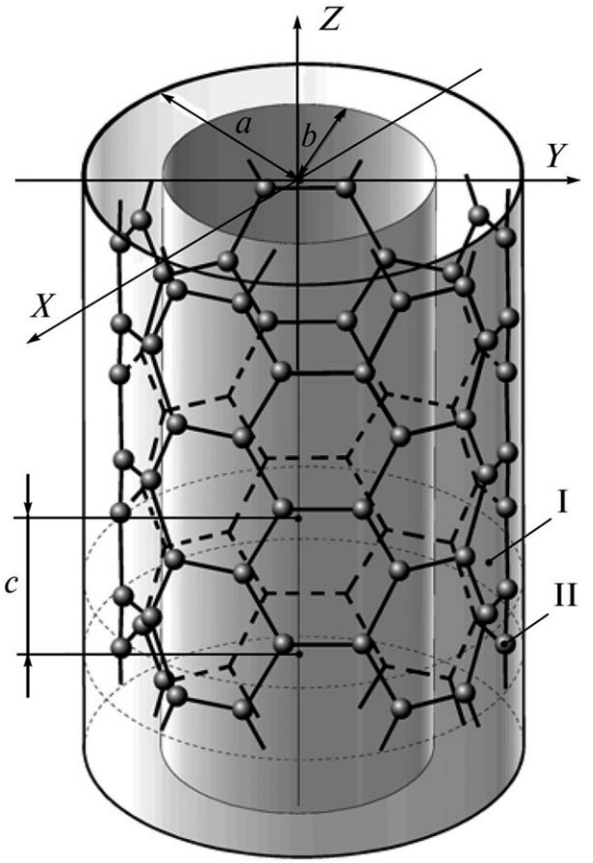

Figure 2. Nanotube in a tubular potential. (Reproduced from Ref. 20, with permission from Springer.).

method, the eigenfunctions $\Psi_{n,k}(\mathbf{r})$ of the Schrödinger equation are the superposition of the basis Ψ^k_{PMN} LACWs taken to be the eigenfunctions of this equation for the interspherical and MT regions. Cylindrical indices *P*, *M*, and *N* are defined in Eqs. 3–6; Moreover, the functions Ψ^k_{PMN} should be continuous together with their first derivatives. In the interatomic region, the LACWs are the solutions of the Schrödinger equation for electron in the tubular potential well. Using the cylindrical coordinate system (Z,Φ,R) and Rydberg units, this equation can be written as

$$\left\{-\left[\frac{1}{R}\frac{\partial}{\partial R}\left(R\frac{\partial}{\partial R}\right)+\frac{1}{R^2}\frac{\partial^2}{\partial\Phi^2}+\frac{\partial^2}{\partial Z^2}\right]+U(R)\right\}\Psi(Z,\Phi,R) =E\Psi(Z,\Phi,R) \tag{1}$$

$$U(R)=\begin{cases}0, & b\le R\le a\\ \infty, & R<b, R>a\end{cases}. \tag{2}$$

The solutions of Eq. 1 with potential (2) can be taken from the text books in quantum mechanics.[25,26] They are the products of three functions

$$\Psi^k_{PMN}(Z,\Phi,R)=\Psi^k_P(Z)\Psi_M(\Phi)\Psi_{MN}(R). \tag{3}$$

The functions

$$\Psi^k_P(Z)=(1/\sqrt{c})\exp[i(k+k_P)Z], k_P=(2\pi/c)P, P=0,\pm1, \pm2,\ldots,-\pi/c\le k\le\pi/c; \tag{4}$$

and

$$\Psi_M(\Phi)=\frac{1}{\sqrt{2\pi}}e^{iM\Phi}, M=0,\pm1,\pm2,\ldots \tag{5}$$

describe the propagation of electrons along the translation axis of tube and their rotation about this axis, respectively. The functions $\Psi_{MN}(R)$ corresponding the radial movement of electrons and depending on the radial quantum number $N=1$, 2,... are solutions of the equation

$$\left[-\frac{1}{R}\frac{d}{dR}R\frac{d}{dR}+\frac{M^2}{R^2}\right]\Psi_{MN}(R) +U(R)\Psi_{MN}(R)=E_{|M|N}\Psi_{MN}(R). \tag{6}$$

Because $U(R)=0$ at $b\le R\le a$, the Eq. 6 takes a form of a Bessel equation

$$\left[\frac{d^2}{dR^2}+\frac{1}{R}\frac{d}{dR}+\kappa^2{}_{|M|,N}-\frac{M^2}{R^2}\right]\Psi_{MN}(R)=0, \tag{7}$$

where $\kappa_{|M|,N}=\{E_{|M|,N}\}^{1/2}$. The solutions of the Eq. 7 are the superposition of the *M*th order cylindrical functions of the first J_M and second Y_M types[27,28]

$$\Psi_{MN}(R)=C^J_{MN}J_M\left(\kappa_{|M|,N}R\right)+C^Y_{MN}Y_M\left(\kappa_{|M|,N}R\right). \tag{8}$$

The constants C^J_{MN} and C^Y_{MN} are chosen from the conditions of normalization and vanishing of the $\Psi_{MN}(R)$ functions at the barriers Ω_a and Ω_b.[18,19,24]

Similar to LAPW technique of solids,[8–11] in the MT regions of atoms α_{MT}, the basis LACWs are expanded in spherical harmonics $Y_{lm}(\theta,\varphi)$ as

$$\Psi^{PMN,k}_{\alpha_{MT}}(\rho,\theta,\varphi)=\sum_{l=0}^{\infty}\sum_{m=-l}^{l}[A^{PMN,k}_{lm,\alpha_{MT}}u_{l,\alpha_{MT}}(\rho,E_{l,\alpha_{MT}}) +B^{PMN,k}_{lm,\alpha_{MT}}\dot{u}_{l,\alpha_{MT}}(\rho,E_{l.\alpha_{MT}})]Y_{lm}(\theta,\varphi). \tag{9}$$

Here, the local spherical coordinates $(r,\theta,\varphi,)$ are used, while the $u_{l,\alpha_{MT}}$ functions are obtained from the atomic radial Schrödinger equation

$$\frac{1}{\rho}\frac{d^2\rho u_{l,\alpha_{MT}}(\rho)}{d\rho^2}+\left(E_{l,\alpha_{MT}}-V_{\alpha_{MT}}(\rho)-\frac{l(l+1)}{\rho^2}\right)u_{l,\alpha_{MT}}(\rho)=0, \tag{10}$$

where $\dot{u}_{l,\alpha_{MT}}=\left[\partial u_{l,\alpha_{MT}}/\partial E\right]_{E_{l,\alpha_{MT}}}$ and $V_{\alpha_{MT}}$ is the electron potential of the atomic α_{MT} sphere. The $A^{PMN,k}_{lm,\alpha_{MT}}$ and $B^{PMN,k}_{lm,\alpha_{MT}}$ coefficients can be calculated from the conditions that the basis functions together with their first derivative are continuous at $\rho=r_{\alpha_{MT}}$. This algebraic problem was solved in the terms of an addition theorem for Bessel functions,[7,18] where the following analytical expressions for coefficients $A^{PMN,k}_{lm,\alpha_{MT}}$ and $B^{PMN,k}_{lm,\alpha_{MT}}$ were obtained

$$A^{PMN,k}_{lm,\alpha_{MT}}=r^2_{\alpha_{MT}}D^{PMN,k}_{lm,\alpha_{MT}}a^{PMN,k}_{lm,\alpha_{MT}}, \tag{11}$$

$$B^{PMN,k}_{lm,\alpha_{MT}}=r^2_{\alpha_{MT}}D^{PMN,k}_{lm,\alpha_{MT}}b^{PMN,k}_{lm,\alpha_{MT}}, \tag{12}$$

with

$$D^{PMN,k}_{lm,\alpha_{MT}}=\frac{1}{\sqrt{2c}}(-1)^{\frac{m+|m|}{2}+l}i^l\left[\frac{(2l+1)(l-|m|)!}{(l+|m|)!}\right]^{1/2} \times\exp\{i(K_PZ_{\alpha_{MT}}+M\Phi_{\alpha_{MT}})\}(-1)^M \times\left[C^J_{MN}J_{m-M}\left(\kappa_{|M,N|}R_{\alpha_{MT}}\right)+C^Y_{MN}Y_{m-M}\left(\kappa_{|M,N|}R_{\alpha_{MT}}\right)\right], \tag{13}$$

$$a^{PMN,k}_{lm,\alpha_{MT}}(r_{\alpha_{MT}})=I^{PMN,k}_{2,lm,\alpha_{MT}}\dot{u}_{l,\alpha_{MT}}(r_{\alpha_{MT}})-I^{PMN,k}_{1,lm,\alpha_{MT}}\dot{u}'_{l,\alpha_{MT}}(r_{\alpha_{MT}}), \tag{14}$$

$$b^{PMN,k}_{lm,\alpha_{MT}}(r_{\alpha_{MT}})=I^{PMN,k}_{1,lm,\alpha_{MT}}u'_{l,\alpha_{MT}}(r_{\alpha_{MT}})-I^{PMN,k}_{2,lm,\alpha_{MT}}u_{l,\alpha_{MT}}(r_{\alpha_{MT}}). \tag{15}$$

Here, $Z_{\alpha_{MT}}$, $\Phi_{\alpha_{MT}}$, $R_{\alpha_{MT}}$ are the cylindrical coordinates of atom α_{MT}, a prime indicates a derivative with respect to the radius ρ, and

$$I^{PMN,k}_{1,lm,\alpha_{MT}}=2\int_0^{\pi/2}\exp\{iK_Pr_{\alpha_{MT}}\cos\theta\}J_m\left(\kappa_{|M|,N}r_{\alpha_{MT}}\sin\theta\right)P^{|m|}_l(\cos\theta)\sin\theta d\theta, \tag{16}$$

$$I^{PMN,k}_{2,lm,\alpha_{MT}}=2\int_0^{\pi/2}\exp\{iK_Pr_{\alpha_{MT}}\cos\theta\}\{iK_P\cos\theta J_m\left(\kappa_{|M|,N}r_{\alpha_{MT}}\sin\theta\right) +0.5\kappa_{|M|,N}\sin\theta\}\left[J_{m-1}\left(\kappa_{|M|,N}r_{\alpha_{MT}}\sin\theta\right)-J_{m+1}\left(\kappa_{|M|,N}r_{\alpha_{MT}}\sin\theta\right)\right] \times P^{|m|}_l(\cos\theta)\sin\theta d\theta, \tag{17}$$

where $P^{|m|}_l$ are the augmented Legendre polynomials. This determines finally the basis $\Psi^k_{PMN}(\mathbf{r})$ functions.

The formulas for the overlap and Hamiltonian matrix elements and solving the secular equation using the LACW basis are presented elsewhere.[7,18,19] As the results, one gets

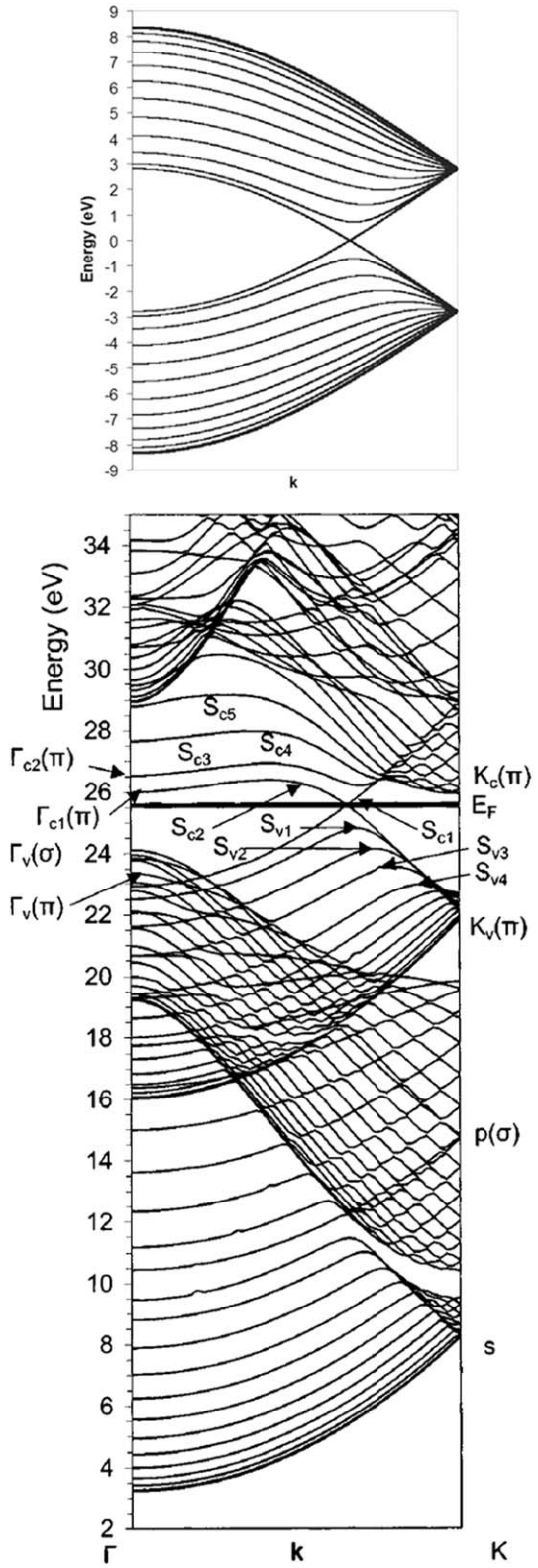

Figure 3. Band structure of (12,12) carbon nanotube calculated using the Huckel (top) and LACW (bottom) methods. (Reproduced from Ref. 29, with permission from American Institute of Physics.).

the energies $E_n(k)$ of electron bands and the eigenfunctions $\Psi_{n,k}(\mathbf{r})$ in form of combinations of the basis $\Psi^k_{PMN}(\mathbf{r})$ functions

$$\Psi_{n,k}(\mathbf{r}) = \sum_{PMN} a^{kn}_{PMN} \Psi^k_{PMN}(\mathbf{r}). \quad (18)$$

As the first example of application, the Figure 3 shows the calculated LACW band structures for the armchair (12,12) carbon nanotube in comparison with similar Hückel data.[18,29] Both the Hückel and LACW dispersion curves show the metal-type zero-gap band structures of this tube with the Fermi level located at the crossing of two dispersion curves at the Brillouin zone point k $\approx$ (2/3)(π/c). However, the LACW calculation gives much more informative band structure, because this method describes not only π-state, but also the inner p_σ and s bands. It takes into account the tubules curvature, sp and $\sigma\pi$ hybridizations, and other effects of which are beyond the Hückel approximations. For example, there are intersections and overlaps of π and σ curves, the highest occupied σ level $\Gamma_v(\sigma)$ being located notably above the highest occupied π level $\Gamma_v(\pi)$.

The dependences of the direct $\sigma\pi^*$ and $\pi\pi^*$ optical transition energies versus the inverse diameter d^{-1} of the (n, n) tubules show significant deviations from the equation $E_g \sim d^{-1}$ predicted by the simple π electron model (Fig. 4). The situation becomes more complicated because of the very close energy values of $\pi\pi^*$ and $\sigma\pi^*$ transitions and the crossing of corresponding curves. For the (3,3) nanotube with very small diameter and strongest $\sigma\pi$ mixing, the S_{c1} singularity coincides with the Fermi level, resulting in great increase of the density of states at this level and superconductivity of nanotube.[29]

Figure 5 shows the electron structures of semiconducting zigzag (13,0) tube calculated using the two methods.[30] Again, the all-electron LACW results display a much more detailed information on the bands, although both methods predict this tubule to be the semiconductor with direct gap at the Γ point. In contrast to the simple π electron model, the diameter dependence of minimum direct $\pi\pi^*$ transition is oscillating

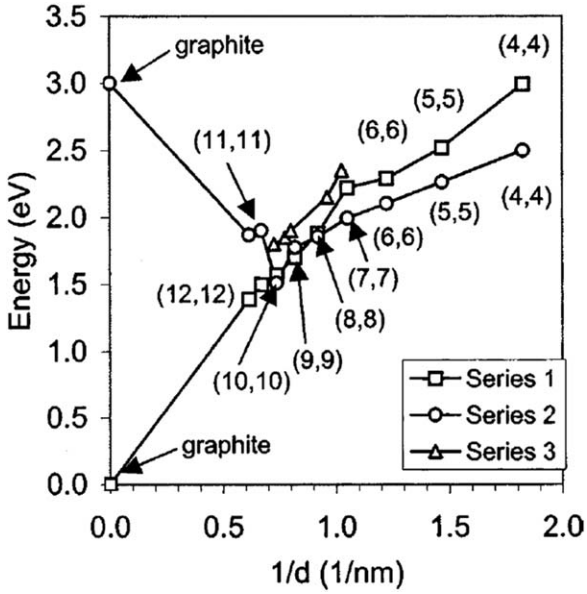

Figure 4. Theoretical direct optical gaps for $\pi\pi^*$ (series 1)and $\sigma\pi^*$ (series 2) transitions in zone center and experimental data (series 3) versus diameters, d, of the (n, n) tubes. (Reproduced from Ref. 29, with permission from American Institute of Physics.).

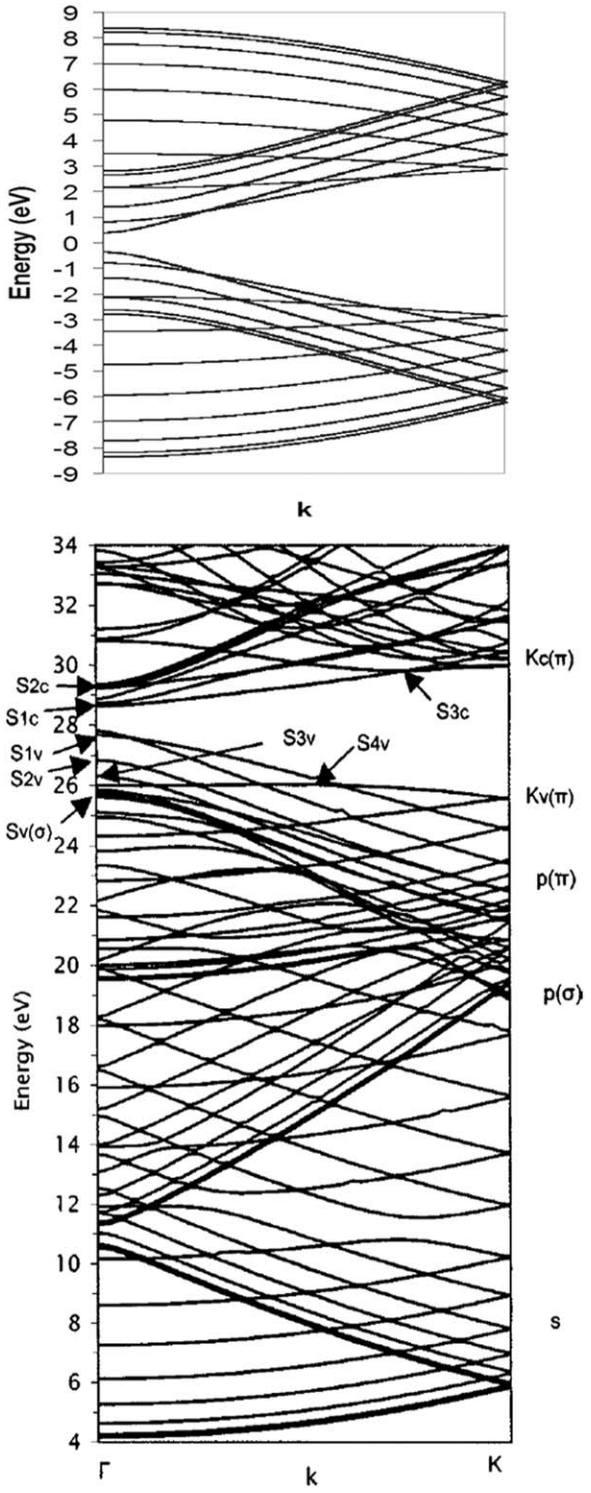

Figure 5. Band structure of (13,0) nanotube calculated using the Huckel (top) and LACW (bottom) methods. (Reproduced from Ref. 30, with permission from American Institute of Physics.).

function with sharp gap reduction at $d < 10$ Å and formation of metallic zigzag nanotubes at $d < 6.5$ Å (Fig. 6).

Chiral Nanotubes

Previous calculations of carbon nanotubes dealt with examples of non-chiral tubules having only small translational cell. For chiral tubes, the translational unit cell are typically very large; for example, there are more than 10^5 atoms in translational cell of the (100,99) tube. Fortunately, all symmetry properties of nanotubes can be taken into account,[12,31,32] the LACW theory of electronic band structure of such tubules can be developed, and the dispersion curves of the tubules like (100,99) can be calculated successfully.

The (n_1,n_2) nanotube has an axis of C_n symmetry, where n is the greatest common factor of n_1 and n_2. Due to the nth order rotational symmetry, one can determine the wave vector k_Φ, and wave functions can be written as follows

$$\Psi\left(Z,\Phi+t\omega_{n,}R\right)=e^{ik_\Phi t\omega_n}\Psi(Z,\Phi,R). \tag{19}$$

with integer t. Substituting $t = n$, we find $k_\Phi = L + nM$; $M = 0, \pm1, \ldots; L = 0, 1, \ldots, n - 1$.

The ideal single-walled nanotubes are also invariant under the screw $\hat{S}(h,\omega)$ translations, which are the displacements

$$h=\frac{3d_{c-c}}{2}\frac{n}{\left(n_1^2+n_2^2+n_1n_2\right)^{1/2}}=\frac{3\sqrt{3d^2_{c-c}}}{4\pi}\frac{n}{R_{NT}}. \tag{20}$$

along the Z axis with rotations

$$\omega=2\pi\frac{n_1p_1+n_2p_2+(n_2p_1+n_1p_2)/2}{n_1^2+n_2^2+n_1n_2} \tag{21}$$

about it. Due to the fact that the screw translations are isomorphous to the group of common translations, one can use the Bloch's theorem and write

$$\Psi(Z+th,\Phi+t\omega,R)=e^{(k+k_P)th}\Psi(Z,\Phi,R). \tag{22}$$

Now, in the Ω_{II} region, the basis functions can be presented as the symmetrized cylindrical waves[13,33,34]

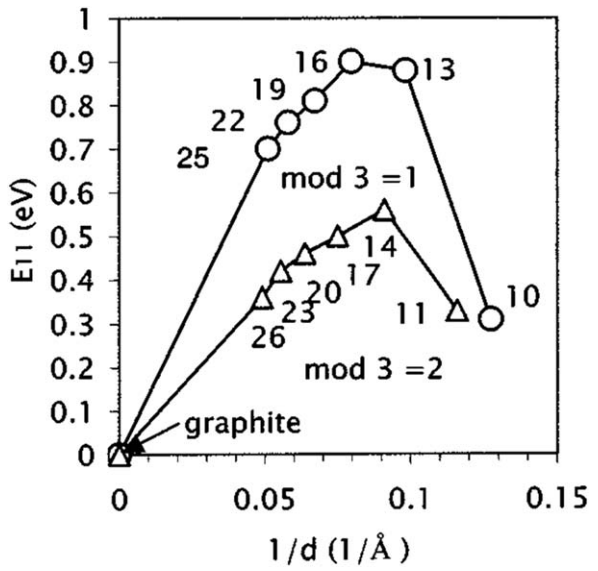

Figure 6. Minimum optical gap E_{11} versus diameter, d, of the semiconducting (0,n) tubules. (Reproduced from Ref. 30, with permission from American Institute of Physics.).

$$\Psi_{II,PMN}(Z,\Phi,R|k,L)=\frac{1}{\sqrt{2\pi h/n}}$$
$$\times\exp i\left\{\left[k+k_P-(L+nM)\frac{\omega}{h}\right]Z+(L+nM)\Phi\right\} \quad (23)$$
$$\times C^{J,L}_{M,N}J_{L+nM}\left(\kappa_{|L+nM|}R\right)+C^{Y,L}_{M,N}Y_{L+nM}\left(\kappa_{|L+nM|}R\right)$$

which are the solution of the Schrödinger equation for the electron in the tubular potential well and satisfy the symmetry properties Eqs. 19, 22. As above, the coefficients $C^{J,L}_{MN}$ and $C^{Y,L}_{MN}$ are found by equating to zero the wave function at the outer and inner cylindrical potential barriers Ω_a and Ω_b as well as from normalization conditions.

The basis functions in the regions of atomic spheres are again expanded in the Y_{lm} series of the linear combination of spherical harmonics Eq. 9. Applying the sewing conditions, we obtain the explicit formulas for basis LACWs, determine the overlap and Hamiltonian integrals, and calculate the dispersion laws for electrons using the secular equation.

Figure 7 shows the band structure of the chiral (11,3) tubule with 652 atoms in the translational unit cell. There is no rotational symmetry in this system. By taking into consideration the screw symmetry of the nanotube, only about 150 basis functions are required for convergence of electronic levels with an accuracy of 0.01 eV and the band structure is seen to be very simple. Particularly, there are only four dispersion curves in a valence band corresponding to the doubly occupied predominantly *s*, $p_{1\sigma}$, $p_{2\sigma}$, and p_π electronic states and only one low-energy unoccupied p_π*-type dispersion curve in the conduction band. (If only translations were taken into account, we would obtain a difficult-to-analyze band structure containing 1304 bands in the valence band and 326 π-bands in the conduction band.) According to the LACW data, the nanotube (11,3) is a semiconductors with the direct energy gaps E_{11} equal to 0.656 at $k=0.24(\pi/h)$.

Another example is the band structure of the chiral (10,5) nanotube having C_5 rotational and screw axes (Fig. 8). Here, the electron bands depend on the two quantum numbers, namely, continuous vector *k* of the screw translations and the rotational integer number $4\geq L\geq 0$. According to LACW data, this nanotube should be the semiconductor with the smallest optical gap equal to 0.58 eV and corresponding to the direct excitation at point $k\approx 0.57(\pi/h)$ for $L=3$. The second one corresponds to the direct transition at $k\approx 0.86(\pi/h)$ for $L=4$ and energy equal to 1.01 eV. For the third gap equal to 1.82 eV the direct excitation takes place at $k\approx 0.28(\pi/h)$ for $L=2$.

As a decisive demonstration of the effectiveness of this version of our method (for the Guinness Book of Records), we calculated the dispersion curves structure of the (100,99) tubule and predicted the semiconducting properties of this system with minimum optical gap equal to 0.04 eV near Brillouin zone center.[13]

Substitutional Impurities

Based on the LACW and Green's function techniques, an *ab initio* method for calculation of the electronic structure of the point substitutional impurities in the nanotubes is developed.[35] In the band structure studies, the central problem is

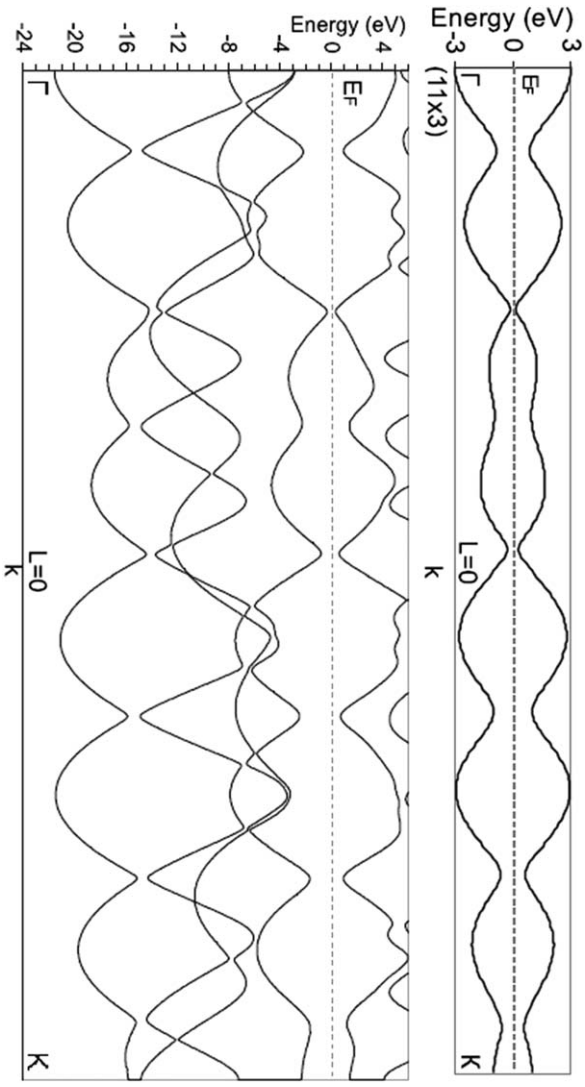

Figure 7. Band structure of the (11,3) tubule calculated using LACW (left) and π electron (right) methods with account of screw symmetry. (Reproduced from Ref. 13, with permission from American Physical Society.).

computation of the wave functions and energies using the Schrödinger equation. However, the calculation of these characteristics can be avoided, if instead the Green's function $G(\mathbf{r},\mathbf{r}';E)$ is determined.[36,37] Particularly, the spectrally and space-resolved density of states can be obtained from the imaginary part of $G(\mathbf{r},\mathbf{r}';E)$ using the following equation

$$\rho(\mathbf{r};E)=-\frac{1}{\pi}\mathrm{Im}G(\mathbf{r},\mathbf{r}';E). \quad (24)$$

For ideal nanotube, in terms of a complete set of the eigenfunctions $\Psi_\lambda(k|r)$ and eigenvalues E_λ(k) calculated using the LACW method, the following spectral representation can be used

$$G(\mathbf{r},\mathbf{r}';E)=\frac{c}{2\pi}\sum_\lambda\int_{-\pi/c}^{\pi/c}\frac{\psi_\lambda(\mathbf{r}|k)\psi^*_\lambda(\mathbf{r}'|k)}{E-E_\lambda(k)+i\varepsilon}dk. \quad (25)$$

to obtain the Green's function $(\varepsilon\rightarrow 0^+)$.

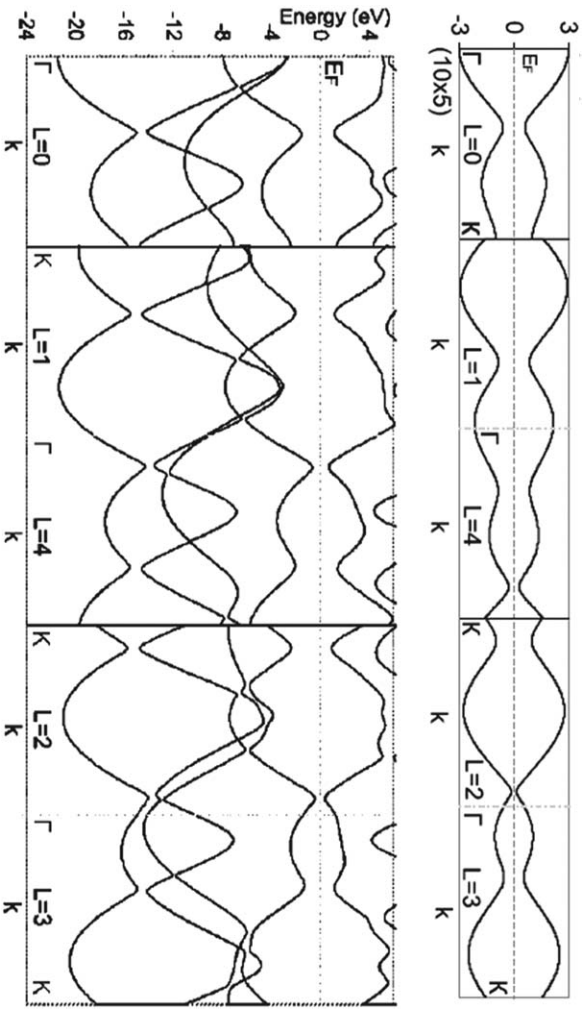

Figure 8. Band structure of the (10,5) tubule calculated using LACW (left) and π electron (right) methods with account of screw and rotational symmetry. (Reproduced from Ref. 13, with permission from American Physical Society.).

In the case of the impurity tubule, the equation for the Green's function $\tilde{G}(\mathbf{r},\mathbf{r}';E)$ can be written as

$$\begin{aligned}&\{\hat{H}-E\}\tilde{G}(\mathbf{r},\mathbf{r}';E)=-\delta(\mathbf{r}-\mathbf{r}')\\&-\Delta V(\mathbf{r})\tilde{G}(\mathbf{r},\mathbf{r}';E).\end{aligned}\tag{26}$$

Here, $\hat{H}$ is the Hamiltonian of the perfect tubule and $\Delta V(\mathbf{r})=\tilde{V}(\mathbf{r})-V(\mathbf{r})$ is a difference between the potentials of the doped and perfect tubes. It follows from this equation that the Green's function $\tilde{G}(\mathbf{r},\mathbf{r}';E)$ corresponding to the new Hamiltonian $\hat{H}+\Delta V(\mathbf{r})$ is related to the Green's function $G(\mathbf{r},\mathbf{r}';E)$ of the $\hat{H}$ operator via the Dyson integral equation

$$\tilde{G}(\mathbf{r},\mathbf{r}';E)=G(\mathbf{r},\mathbf{r}';E)+\int G(\mathbf{r},\mathbf{r}'';E)\Delta V\left(\mathbf{r}''\right)\tilde{G}(\mathbf{r}'',\mathbf{r}';E)d\mathbf{r}''.\tag{27}$$

Most important is that the perturbed potential $V(\mathbf{r})$ is well localized near the impurity center.

For array of the spherically symmetric nonoverlapping potentials, the Green's function is defined via

$$\begin{aligned}&\{-\Delta+V_{n\alpha}(\mathbf{r})-E\}G(\mathbf{r}+\mathbf{R}_{n\alpha},\mathbf{r}'+\mathbf{R}'_{n'\alpha'};E)=\\&-\delta_{n\alpha,n'\alpha'}\delta(\mathbf{r}-\mathbf{r}').\end{aligned}\tag{28}$$

One can represent the solutions of this equation as a series expansion in spherical harmonics[38–41]

$$\begin{aligned}&G(\mathbf{r}+\mathbf{R}_{n\alpha},\mathbf{r}'+\mathbf{R}_{n'\alpha'};E)=\\&-i\delta_{n,n'}\delta_{\alpha,\alpha'}\sqrt{E}\sum_L u_l^{n\alpha}(r_<,E)Y_L(\hat{\mathbf{r}})H_l^{n\alpha}(r_>,E)Y_L^*(\hat{\mathbf{r}}')\\&+\sum_{L,L'}u_l^{n\alpha}(r,E)Y_L(\hat{\mathbf{r}})G_{L,L'}^{n\alpha,n'\alpha'}(E)u_{l'}^{n'\alpha'}(r',E)Y_{L'}^*(\hat{\mathbf{r}}').\end{aligned}\tag{29}$$

Here, $L=(l,m)$ are the orbital quantum numbers, $r_<=\min(r,r')$, $r_>=\max(r,r')$, $G_{L,L'}^{n\alpha,n'\alpha'}(E)$ are the energy-dependent coefficients of expansion,

$$H_l^{n\alpha}(r,E)=u_l^{n\alpha}(r,E)+iN_l^{n\alpha}(r,E),\tag{30}$$

the $u_l^{n\alpha}(r,E)$ and $N_l^{n\alpha}(r,E)$ are the regular and irregular solutions of radial equation 10. In each MT sphere, the expansion (29) satisfies the general Schrödinger Eq. 27, and the structural Green's function $G_{L,L'}^{n\alpha,n'\alpha'}(E)$ describes the connection of the solutions in the different spheres. In this way, the multiple-scattering problem is reduced to the solution of an algebraic problem.

Comparison of Eqs. 27 and 29 allows us to calculate the matrix elements of the Green function $G_{L,L'}^{n\alpha,n'\alpha'}(E)$ for an ideal nanotube. If they are known, the structural Green's function $\tilde{G}_{L,L'}^{n\alpha,n'\alpha'}(E)$ for the impurity nanotube can be calculated using a matrix Dyson equation

$$\begin{aligned}&\tilde{G}_{L,L'}^{n\alpha,n'\alpha'}(E)=G_{L,L'}^{n\alpha,n'\alpha'}(E)+\\&\sum_{n'',\alpha''}\sum_{L''}G_{L,L''}^{n\alpha,n''\alpha''}(E)\Delta t_{l''}^{n''\alpha''}(E)\tilde{G}_{L'',L'}^{n''\alpha'',n'\alpha'}(E).\end{aligned}\tag{31}$$

Here,

$$t_l^{n\alpha}(E)=\int_0^{r_{n\alpha}}j_l\left(\sqrt{E}r\right)V_{n\alpha}(r)u_{l,n\alpha}\left(r,E_{l,n\alpha}\right)r^2dr\tag{32}$$

is a scattering t matrix for the potential $V_{n\alpha}(r)$, and $\Delta t_{l''}^{n''\alpha''}(E)=\tilde{t}_{l''}^{n''\alpha''}-t_{l''}^{n''\alpha''}$ is a difference between the t matrices of the doped and perfect nanotubes. Since this difference is restricted to the region of the impurity, the Green's function can be determined in real space by matrix inversion, the rank of which $n_d(l_{\max}+1)^2$ depends on the number n_d of perturbed MT potentials and maximum angular momentum $l_{\max}$ used in expansion (19). For the single impurities studied, we use a single-site approximation that is we neglected the perturbations of potentials of the host atoms surrounding the impurity.

Substituting the $\tilde{G}_{L,L'}^{n\alpha,n'\alpha'}(E)$ to Eq. 29, we obtain the Green's function $\tilde{G}(\mathbf{r},\mathbf{r}';E)$ for calculating the electron properties of the nanotube with impurity. In work,[35] we apply this technique to the particular case of local electronic density of states in the

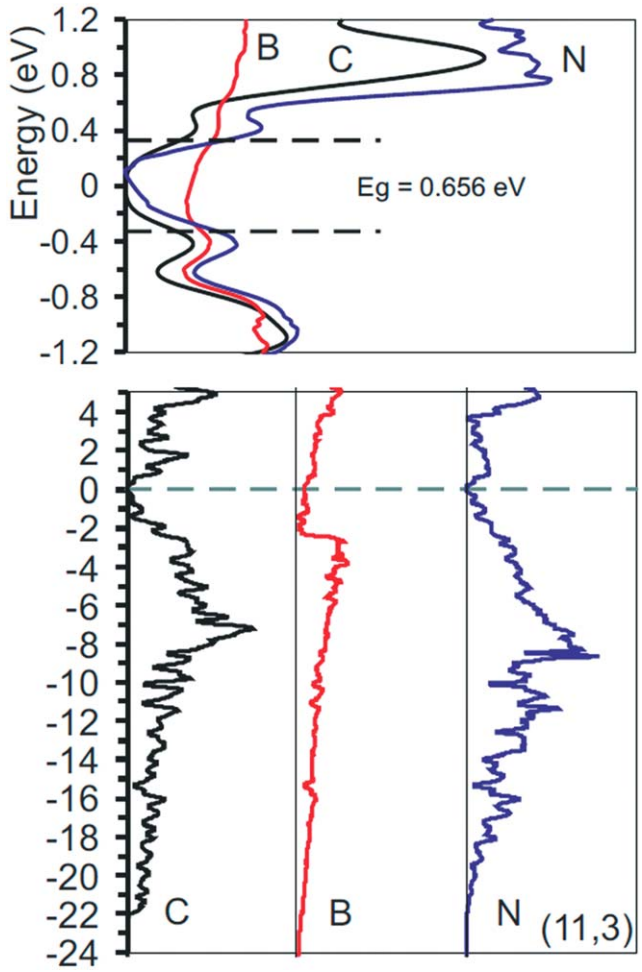

Figure 9. Local density of states of the perfect (C) and boron (B) and nitrogen (N) doped chiral semiconducting (11,3) nanotube. (Reproduced from Ref. 35, with permission from American Physical Society).

regions of the impurity B and N atoms in the carbon nanotubes having different geometries and electron spectra.

Figure 9 exhibits the effects of substitutional impurities on the density of states of chiral (11,3) tubule. There is a great difference between the effects of the donor and acceptor impurities in the vicinity of optical gap. The boron-related states clearly close the optical gap of the perfect nanotubes. The influence of nitrogen impurity is limited with a small growth of the local density of states below and above the E_F. This is also truth for other doped semiconducting tubules investigated.[35]

In the Fermi region of purely metallic carbon (5,5) tubule, the electronic structure is also significantly affected by impurities (Fig. 10), but both defects do not break the metallic zero-gap type of density of states. An impurity-induced increase of the density of states is the main perturbation of electron properties of all tubules having the metallic band structures.

Double-Walled Nanotubes

There are the two tubules (inner and outer) in a double-walled carbon nanotube with van der Waals type coupling between them. Sometimes such nanotubes are considered as the nanomaterial analogs of coaxial cables. Although, the chemical bonding of the inner and outer concentric cylindrical layers is weak, a tunneling exchange of electrons between them is possible and can perturb the electron properties of such nanocables. In the terms of LACW and MT approximations, these effects were studied in works.[42,43]

The sense of MT approach to the double-walled systems should be clarified. Actually, to account for the effects of electron tunneling, we assume that the potential barriers Ω_{a1} and Ω_{b2} between the individual tubules are high, but finite (Fig. 11). The constant potential V_f in the classically forbidden region Ω_f, the same for all nanotubes, was selected using the data on the bulk graphite band structure, in which the interlayer coupling effects are observed as the splittings and shifts of the band curves by a couple of eV.[44]

For the potential shown in the Fig. 11, the solutions of the Schrödinger equation can be found as follows. In the region Ω_f between the two tubules and in interatomic space $\Omega_{II,j}$ of two tubes ($j = 1, 2$), the wave functions are obtained again from the Eq. 1 written using the cylindrical coordinates, but the electron potential $U(R)$ has now a somewhat more sophisticated form

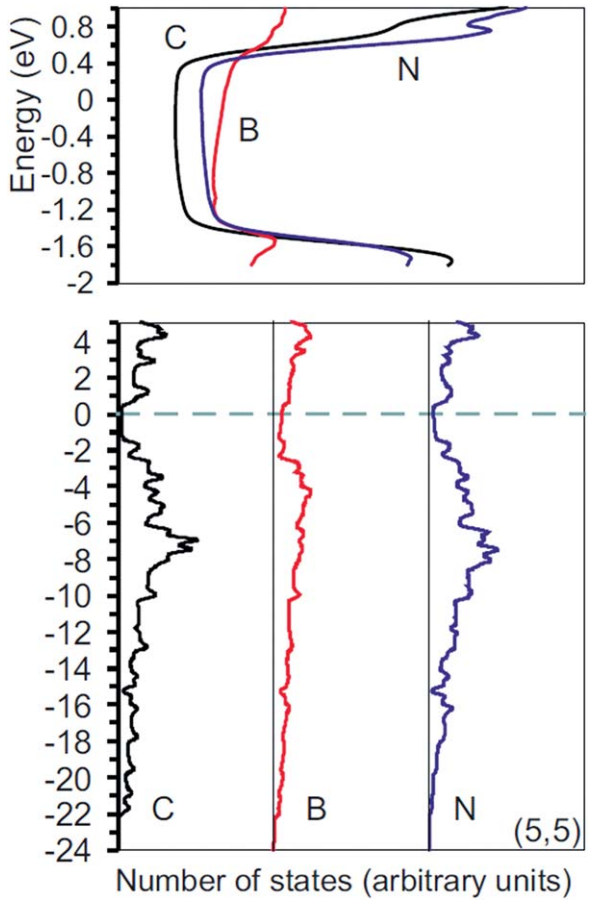

Figure 10. Local density of states of the perfect (C) as well as boron (B) and nitrogen (N) doped achiral metallic (5,5) nanotube. (Reproduced from Ref. 35, with permission from American Physical Society).

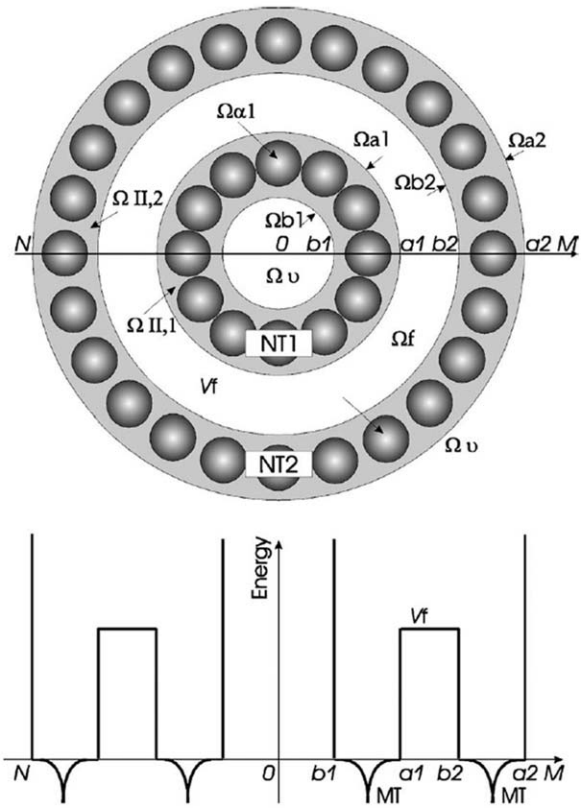

Figure 11. Cross section of double-walled nanotube and potential energy profile. (Reproduced from Ref. 42, with permission from American Physical Society.).

$$U(R)=\begin{cases}0, & b_1 \le R \le a_1, b_2 \le R \le a_2\\ \infty & R < b_1, R > a_2\\ V_F, & a_1, \le R \le b_2\end{cases}. \qquad (33)$$

Because of the rotational symmetry of the potential $U(R)$, the product $\Psi(Z,\Phi,R) = \Psi^k_P(Z)\Psi_M(\Phi)\Psi_{MN}(R)$ provides again the basis function in these space. For the $\Omega_{II,j}$, where the potential $U(R) = 0$, the radial functions are the same as for the isolated tubules Eq. 8

$$\Psi^j_{II,MN}(R)=C^{J,j}_{MN}J_M\left(\kappa_{|M|,N}R\right)+C^{Y,j}_{MN}Y_M\left(\kappa_{|M|,N}R\right), \qquad (34)$$

and in the intertube space Ω_f, where $U(R) = V_f$, the $\Psi_{f,MN}(R)$ functions are the solutions of the following equation

$$\left[\frac{d^2}{dR^2}+\frac{1}{R}\frac{d}{dR}+\left(V_f-\kappa^2_{|M|,N}\right)-\frac{M^2}{R^2}\right]\Psi_{f|M|,N}(R)=0. \qquad (35)$$

We are interested in the electronic band states of a double-walled nanotube located below the potential V_f of the classical forbidden region ($V_f > \kappa^2_{|M|,N}$), where Eq. 35 takes a form of modified Bessel equation, the solutions of which are superposition of modified Bessel functions of the first K_M and second I_M kinds

$$\Psi_{f|M|,N}(R)=C^k_{M,N}K_M\left(\kappa^f_{|M|,N}R\right)+C^k_{M,N}I_M\left(\kappa^f_{|M|,N}R\right), \qquad (36)$$

where $\kappa^f_{|M|,N}=\left(V_f-\kappa^2_{|M|,N}\right)^{1/2}$. The function $\Psi_{IIf,MN}(R)$ must be equal to zero at $R = a_2$ and $R = b_1$, be continuous and differentiable at $R = a_1$ and $R = b_2$ and normalized that determines the coefficients $C^{J,j}_{MN}$ and $C^{Y,j}_{MN}$ ($j = 1, 2$), C^K_{MN}, C^I_{MN}, $\kappa_{|M|,N}$, and finally the form of the functions $\Psi_{f,MN}(R)$. As before, in the atomic spheres α_{MT} of each tubule, the basis Ψ^k_{PMN} functions of nanotube are expanded in series of $Y_{l,m}$ harmonics Eq. 9 with the A_{lm} and B_{lm} coefficients selected to provide continuity and differentiability of the LACWs on the MT borders. The final results for the double-walled systems including the overlap and Hamiltonian matrix elements can be found in paper,[42] where the total band structures and densities of states in the gap regions were computed for about 20 commensurate semiconducting zigzag and metallic armchair nanotubes, in which the distance between the walls is almost identical to distance between the graphite layers.

Figures 12 and 13 show the examples of calculated results for the (13,0)@(22,0) and (5,5)@(10,10) systems, respectively. One can see that intertube coupling causes the changes of bands, which manifests itself as the shifts in the positions and intensities of peaks and gaps of the inner and outer tubules. However, tunneling of electrons between the nested tubules does not destroy the semiconductor or metallic type of system.

Embedded Nanotubes

In paper,[45] the samples of nanotubes embedded into semiconductor epitaxial layers were obtained and the electrical conductivity of nanotubes in such conditions were measured. This work motivated our LACW simulation of the electronic properties of nanotubes embedded in an infinite solid matrix.[46,47]

Figure 14 shows schematically the model of nanotube in the matrix and the potential energy profile. The matrix is considered as a homogeneous structureless medium with large, but finite constant potential V_m. In this model, a possible formation of chemical bonds between the tubule and matrix was neglected, and the role of the crystal matrix was limited by possibility of delocalization of electrons of nanotubes into the matrix area.

From the computational point of view, this model of nanotube immersed in the unlimited matrix with potential

$$U(R)=\begin{cases}0, & b_1 \le R \le a\\ \infty, & R < b\\ V_m, & R > b\end{cases}. \qquad (37)$$

is even somewhat simpler than the case of double-walled tube with potential Eq. 33.

In the Ω_m region, where $U(R) = V_m$ with V_m located noticeably above the Fermi level, the functions

$$\Psi_{MN}(R)=C^K_{MN}K_M(\kappa^K_{|M|N}R), \qquad (38)$$

are obtained from the Eq. 23 at $V_m, > \kappa^2_{|M|,N}$ and up to a constant factor coincides with modified Bessel of the second kind. Here,

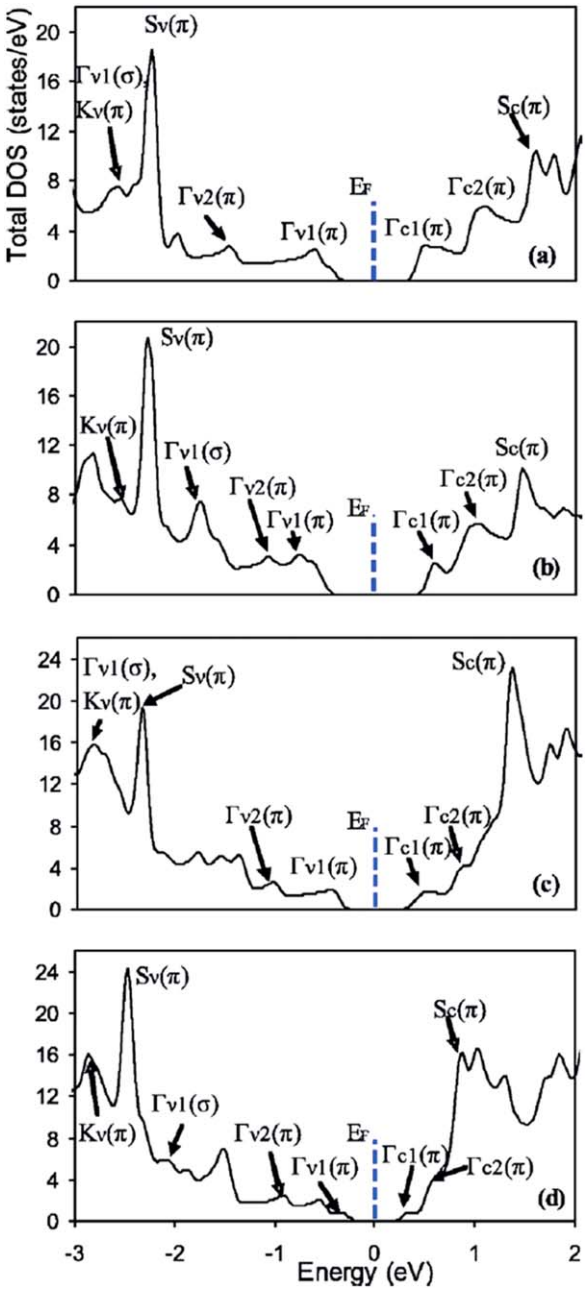

Figure 12. Electron density of states in the gap regions of semiconducting nanotubes: (a) single-walled (13,0) tubule, (b) core (13,0) tubule positioned within (22,0) tubule, (c) single-walled (22,0) tubules, (d) shell (22,0) tubule having inside (13,0) tubule. (Reproduced from Ref. 42, with permission from American Physical Society).

$$\kappa^{K}_{|M|,N} = \left(V_m - \kappa^{2}_{|M|,N}\right)^{1/2}. \tag{39}$$

In the interspherical and MT regions of nanotube, the basis functions are determined by previous Eqs. 3 and 9. They can be sewn together with the solutions (25) that finally determines the overlap and Hamiltonian integrals given in elsewhere.[47]

Figures 15 and 16 show the calculated electron bands near the Fermi level of the metal (5,5) and semiconductor (13,0) nanotubes depending on the dimensionless parameter ε_m, which characterizes the position of the electron potential of the matrix regarding the potential of the nanotubes interspherical area. In both cases, the matrix has a significant impact on the electronic levels of tubes. In metal tube, the σ valence state Γ_{v1} of the Brillouin center are displaced in the

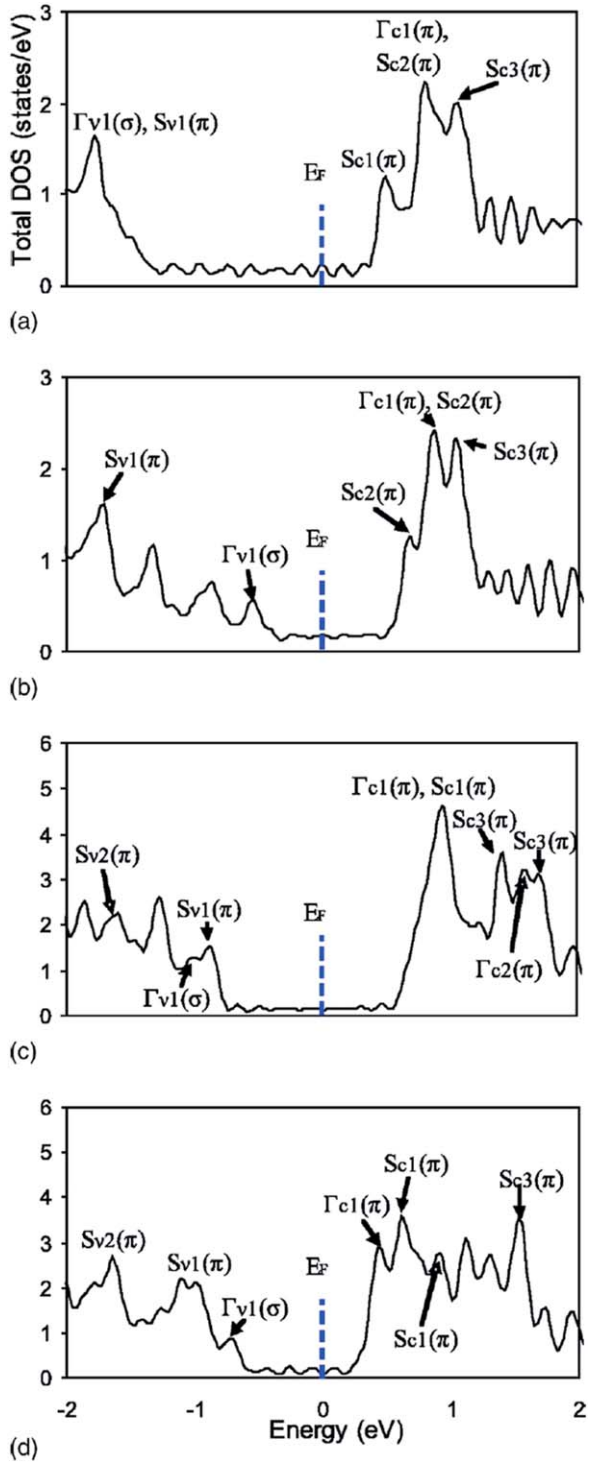

Figure 13. Electron density of states in the Fermi level region for metallic nanotubes: (a) and (c) single-walled (5,5) and (10,10) nanotube; (b) core (5,5) positioned within (10,10) tube; (d) shell (10,10) tube with inside (5,5) tube. (Reproduced from Ref. 42, with permission from American Physical Society).

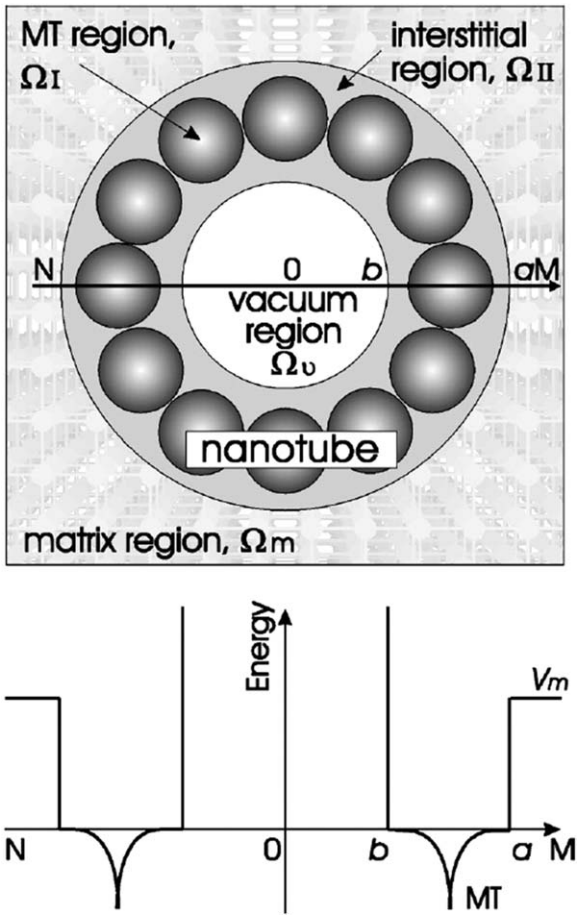

Figure 14. Nanotube positioned into a bulk material and potential energy profile. (Reproduced from Ref. 46, with permission from American Physical Society.).

direction of the conduction band, which leads to growth of the density of states and the appearance of a peak at the Fermi level. The metallic nature of the electronic structure of nanotubes is not destroyed and, even more, an intrinsic electronic conductivity of nanotube should increase due to the increase in number of the free electrons.

In the semiconductor nanotubes, the changes of the electronic properties are more pronounced. Figures 16 and 17 show that lowering of potential of the matrix and an appropriate increase in the spatial delocalization of the electrons of tubule lead to a sharp reduction and closing of the optical gap, with the result that its semiconducting properties are replaced with metallic ones. The predicted metallization of semiconducting carbon nanotubes due to their introduction into the solid environment is consistent with experimental data, according to which any one of the twenty samples with nanotubes in the epitaxial layers have been recorded to be semiconductor, they were all metal.

Atomic Nanowires

The possibility of filling of the interior of nanotubes with metals as shown in Figure 18 greatly expands their scope of application.

The above nanofilament structure are designated as M@nanotube. In the atomic nanowires, the electron motion is confined to cylindrical region with only one (outer) impenetrable cylindrical barrier Ω_a, the radius of which is the same as in pure undoped nanotubes. The potential in the interatomic region is

$$U(R)=\begin{cases}0, & R\le a\\ \infty, & R\ge a\end{cases}. \tag{40}$$

The function $\Psi_{MN}(R)=C^J_{MN}J_M\left(\kappa_{|M|,N}R\right)$ corresponding to the radial movement of electron in the interspherical regions Ω_{II} of the nanofilament depends on the cylindrical Bessel functions of the first J_M kind only. From the algebraic point of view, the problem of nanofilaments without inner vacuum region with potential Eq. 40 is somewhat simpler than problems of nanotubes. It was studied in the papers[6,7] and applied to the atomic

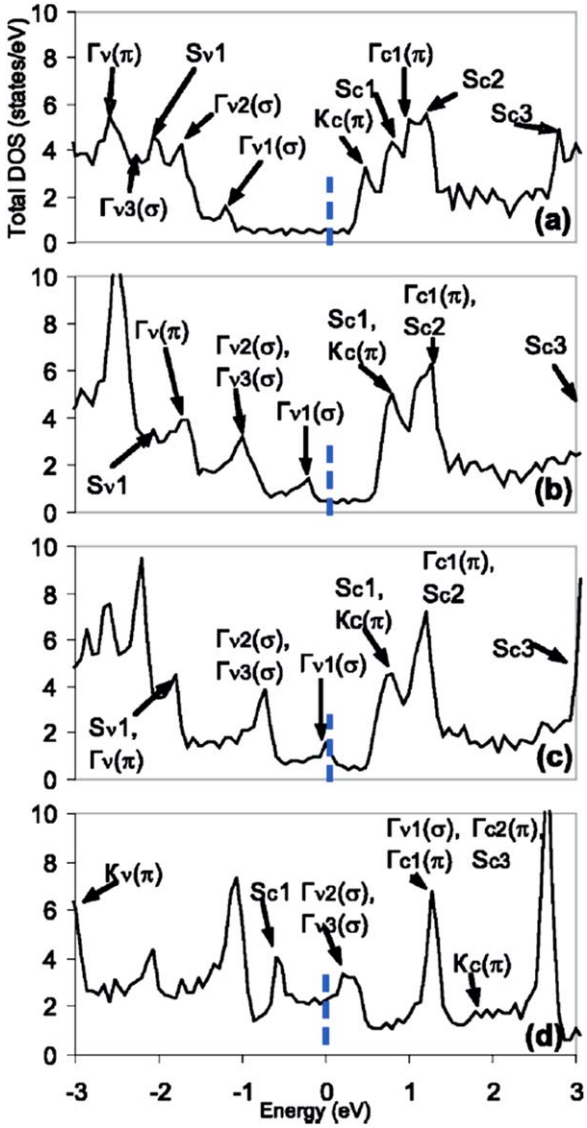

Figure 15. Density of states of the single-walled (5,5) nanotube embedded into a crystal matrix for different barriers; (a) $\varepsilon_m=\infty$ nonembedded tubule; (b–d) $\varepsilon_m=6$, 4, and 2, respectively. (Reproduced from Ref. 46, with permission from American Physical Society).

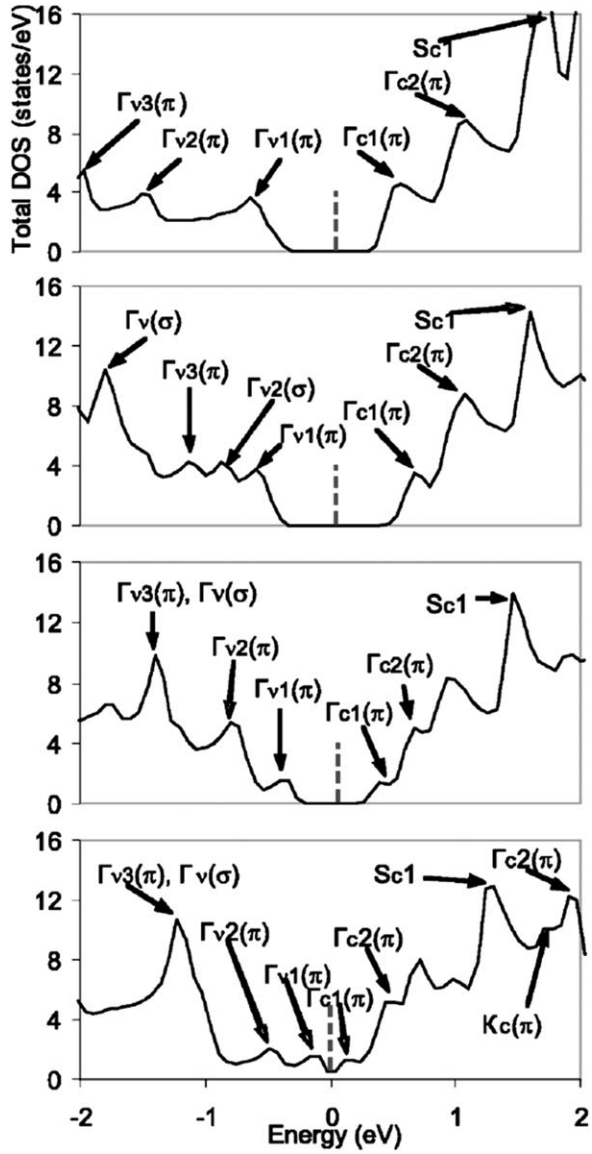

Figure 16. Density of states of the single-walled (13,0) nanotube embedded into a crystal matrix for different barriers; (a) $\varepsilon_m = \infty$ nonembedded tubule; (b–d) $\varepsilon_m = 6$, 4, and 2, respectively. (Reproduced from Ref. 46, with permission from American Physical Society.).

nanowires[19] and nanotubes filled with 3*d* metals.[48,49]Figures 19 and 20 show the total and partial densities of states of electrons in the armchair Cu_n@(5,5) carbon nanotube intercalated with one, two, three, and four copper atoms per translation unit cell. The Fermi level of the pure carbon nanotube is located in the dip of the plot of density of states versus energy; as a result, the density of states at the Fermi level is low that can restrict the electrical conductivity of such a tubule. The introduction of copper atoms dramatically changes the pattern; the dip at the Fermi level is filled, and the electron concentration at the Fermi level increases by an order of magnitude. In the Cu_n@(5,5) compounds with $n = 3$ and $n = 4$, the Fermi level coincides with the peak of the density of states.

The partial densities of states (Fig. 20) show that this dip is filled by both the metal *d* and the carbon p electrons; the metal *d* and carbon p electrons are equally involved in electron transfer in intercalated wires. The introduction of copper not only affects the conducting state of the carbon nanotube but also changes the whole pattern of the valence band of the nanotube, in particular, it increases the valence band width by 5–10 eV due to the low-energy shift of the 2*s*(C) states.

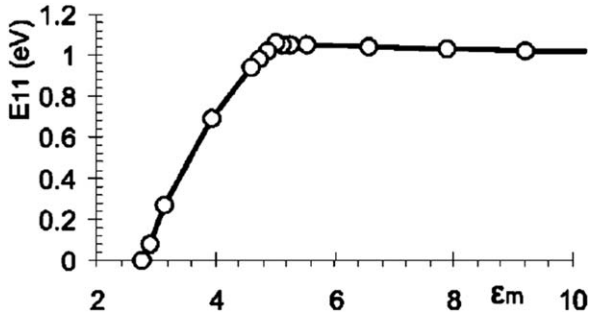

Figure 17. Minimum energy gap E_{11} versus ε_m for a (13,0) nanotube. (Reproduced from Ref. 46, with permission from American Physical Society.).

Spin-Orbit Coupling

Theoretical and experimental studies of a coupling of the electrons spin and their orbital motion is subject of great interest. Because of the cylindrical geometry of the nanotubes, the electron π-states located near the Fermi region can be considered as the clockwise and anticlockwise electron orbits encircling the tube. In the absence of a spin-orbit (SO) interaction, the double orbital and double spin degeneracy should yield the fourfold degenerate electronic levels. In papers,[50,51] we calculated the SO gaps in the Fermi energy region for the metallic (*n*, *n*) tubules and for the metallic and semiconducting linear carbon chains (carbynes). These cases are very interesting, because a formation of gap between the occupied and unoccupied bands is purely relativistic effect here. To obtained a relativistic version of LACW theory, we use the simple two-component relativistic Hamiltonian[14,52,53]

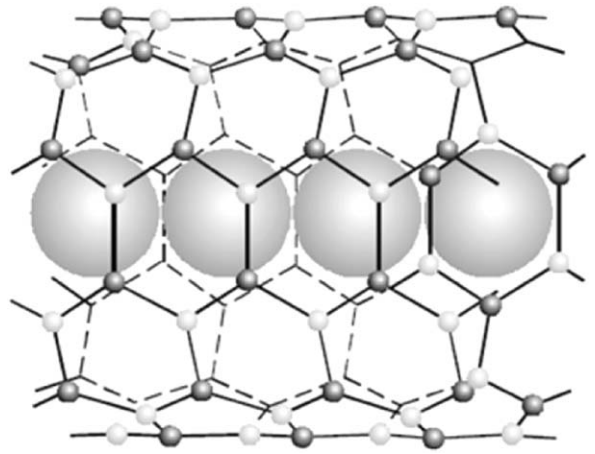

Figure 18. Structure of intercalated nanotube. (Reproduced from Ref. 48, with permission from Springer.).

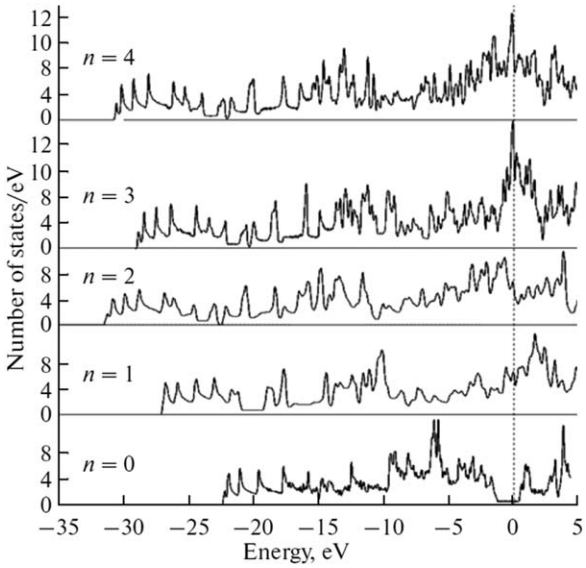

Figure 19. Total densities of states in Cu_n@(5,5) nanotubes with $n = 0,1,2,3$, and 4. The energies are referenced to the Fermi level. (Reproduced from Ref. 48, with permission from Springer.).

$$H = \frac{p^2}{2m} + V + \frac{\hbar}{4m^2c^2}\boldsymbol{\sigma} \cdot [(\nabla V) \times \mathbf{p}]. \tag{41}$$

Here, c is the velocity of light and σ is the Pauli matrix.

The sum $H_0 = p^2/(2m) + V$ is the nonrelativistic operator used above and the third term of the Hamiltonian is the familiar SO coupling operator, which may perturb the nonrelativistic band picture. Because the nonrelativistic terms make the main

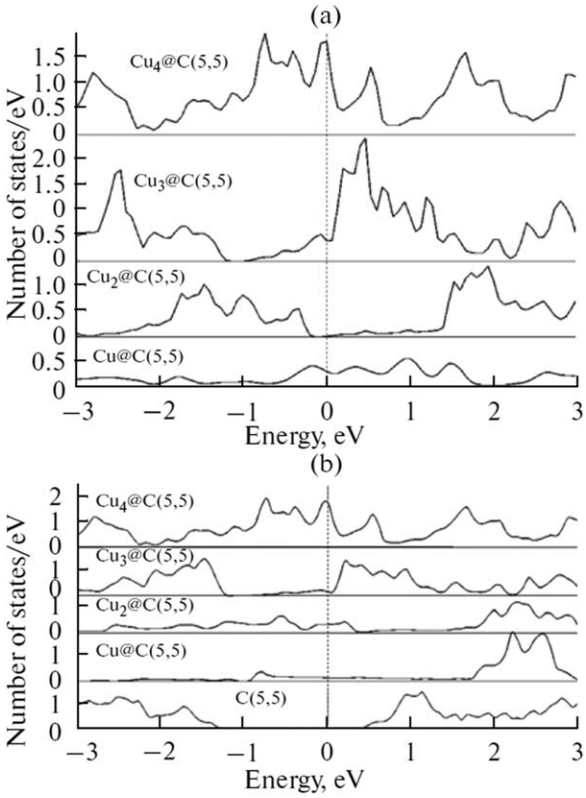

Figure 20. Partial densities of states of (a) copper d electrons and (b) carbon p electrons. (Reproduced from Ref. 48, with permission from Springer.).

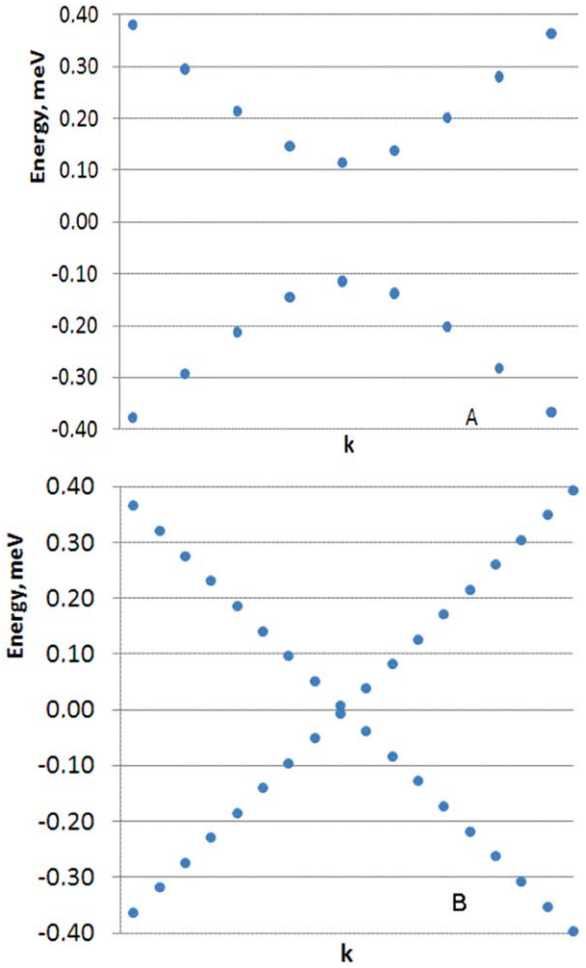

Figure 21. LACW bands of (5,5) nanotube calculated for Fermi energy region with (above) and without (below) spin-orbit coupling. (Originally published under a CC BY-NC-SA license by IOP Publishing. Reproduced from Ref. 50, with permission from Institute of Physics).

contribution to the energy, we use the perturbation procedure. Initially, the eigenvalues $E_n{}^0(k)$ and eigenfunctions

$$\Psi^0_{n,k}(\mathbf{r}) = \sum_{PMN} a^{kn}_{PMN} \Psi^k_{PMN}(\mathbf{r}). \tag{42}$$

of the H_0 are found. Then, using the pure spin functions α and β, the spinor basis partners $\Psi^0_{n,k}(\mathbf{r})\alpha$ and $\Psi^0_{n,k}(\mathbf{r})\beta$ are formed. The matrix elements of the SO part between the spinor basis functions are calculated, and the resulting secular matrix is diagonalized to determine the relativistic energies and functions.

Outside the MT spheres, the $\nabla V = 0$. Due to the spherical symmetry of the $V_{\alpha_{MT}}(\rho)$, the SO operator can be written as[14]

$$\begin{aligned} H_{S-O} &= \frac{1}{c^2}\boldsymbol{\sigma} \cdot [(\nabla V_{\alpha_{MT}}) \times \mathbf{p}] = \frac{1}{c^2}\frac{1}{\rho}\frac{dV_{\alpha_{MT}}}{d\rho}\boldsymbol{\sigma}\mathbf{L} \\ &= \frac{1}{c^2}\frac{1}{\rho}\frac{dV_{\alpha_{MT}}}{d\rho}\left(\frac{1}{2}\sigma_+ L_- + \frac{1}{2}\sigma_- L_+ + \sigma_z L_z\right), \end{aligned} \tag{43}$$

where

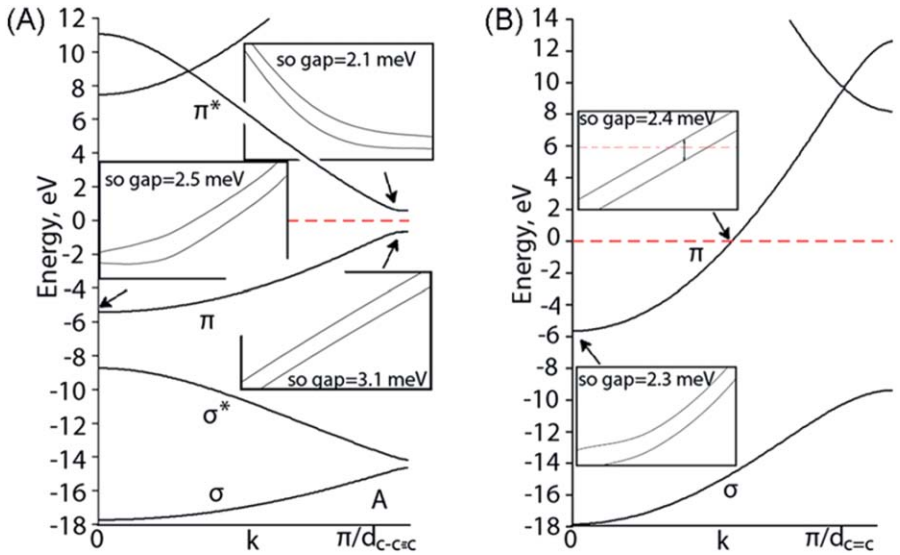

Figure 22. Band structure of polyynic $(\ldots{-}C{\equiv}C{-}C{\equiv}C{-}\ldots)_n$, (A) and cumulenic $(\ldots{=}C{=}C{=}\ldots)_n$ (B) carbon chains calculated with account of SO interaction. (Reproduced from Ref. 51, with permission from American Chemical Society).

$$\sigma_+\alpha = 0,\ \sigma_-\alpha = 2\beta,\ \sigma_z\alpha = \alpha,\ \sigma_+\beta = 2\alpha,\ \sigma_-\beta = 0,\ \sigma_z\beta = -\beta. \quad (44)$$

$$L_z Y_{lm}(\theta\varphi) = mY_{lm}(\theta\varphi), \quad (45)$$

$$L_\pm Y_{lm}(\theta\varphi) = [l(l+1) - m(m\pm1)]^{1/2} Y_{lm\pm1}(\theta\varphi), \quad (46)$$

The L_z, $L_\pm$ operators do not perturb the radial part of the wave function, and the integral $\langle \Psi^k_{P_2M_2N_2}(\mathbf{r})\chi_2 | H_{S-O} | \Psi^k_{P_1M_1N_1}(\mathbf{r})\chi_1 \rangle$ takes the form of product of the radial and angular parts simplifying calculation of these matrix elements, which are presented in papers.[50,51]

Figure 21 shows the dispersion curves bands of the (5,5) nanotube for the Fermi level region calculated with and without SO interaction. In the absence of SO interaction, the occupied π-bonding and unoccupied π*-antibonding states cross near $k = 2\pi/(3d)$, but the SO coupling opens the gap equal to 0.2 meV and the metallic character of nanotube band structure is destroyed. Each energy curve still has the double spin degeneracy, because achiral (5,5) nanotube has the inversion symmetry and the SO interaction does not break the time-reversal symmetry.

Figure 22 shows the SO coupling effects in the band curves of the carbynes. In the absence of SO interaction, the π bands would be fourfold degenerate ones. In a metallic cumulenic carbon chain $(\ldots{=}C{=}C{=}\ldots)_n$, SO splitting of π band is equal to 2.4 meV. In the polyynic semiconducting $(\ldots{-}C{\equiv}C{-}C{\equiv}C{-}\ldots)_n$ chain, the SO gaps are different for the highest occupied and lowest unoccupied states (3.1 and 2.1 meV, respectively). The larger curvature of electron orbits encircling the monoatomic chains as compared with carbon nanotubes results in the larger SO gaps.

Conclusions

In this review paper, the main ideas of the LACW method are summarized. In conclusion, for the sake of completeness, we note that the LACW method was also used previously to calculate the electronic properties of the non-carbon inorganic compounds: the single-atom width transition metal chains,[54] the pristine SiC,[55] BN,[56] BC_2N, and GaAs[57] nanotubes, the segmented nanotubes composed of the alternating layers of BN and SiC nanotubes,[58] the BN nanotubes intercalated with transition metals,[56,59] the BN tubes with the intrinsic N_B and B_N defects and with isoelectronic substitutional impurities P_N, As_N, Sb_N, In_B, Ga_B, and Al_B.[60–62] The calculations of non-carbon systems do not require any new methodical receptions, so we will not focus on these studies in more detail. We hope that we managed to convince the reader that the use of cylindrical waves for the nanotubes offers the obvious advantages in the studies of their properties.

Keywords: nanotubes · augmented cylindrical waves · band structure

How to cite this article: P. N. D'yachkov. *Int. J. Quantum Chem.* **2016**, *116*, 174–188. DOI: 10.1002/qua.25000

[1] S. Iijima, *Nature* **1991**, *354*, 56.
[2] J. W. Mintmire, B. I. Dunlop, C. T. White, *Phys. Rev. Lett*. **1992**, *68*, 631.
[3] R. Saito, M. Fujita, G. Dresselhaus, M. S. Dresselhaus, *Appl. Phys. Lett*. **1992**, *60*, 2204.
[4] R. Saito, M. Fujita, G. Dresselhaus, M. S. Dresselhaus, *Phys. Rev. B*. **1992**, *46*, 1804.
[5] N. Hamada, S. Sawada, A. Oshiyama, *Phys. Rev. Lett*. **1992**, *68*, 1579.
[6] P. N. D'yachkov, O. M. Kepp, A. V. Nikolaev, *Macromol. Symp*. **1998**, *136*, 17.
[7] P. N. D'yachkov, O. M. Kepp, A. V. Nikolaev, *Dokl. Chem*. **1999**, *365*, 67.
[8] J. C. Slater, *Phys. Rev*. **1937**, *51*, 851.
[9] J. C. Slater, The Self-Consistent Field for Molecules and Solids, Quantum Chemistry of Molecules and Crystals, Vol. *4*; McGraw-Hill: New York, **1974**.
[10] O. K. Andersen, *Phys. Rev. B* **1975**, *12*, 3060.
[11] D. D. Koelling, G. O. Arbman, *J. Phys. F: Met. Phys*. **1975**, *5*, 2041.

[12] C. T. White, D. H. Robertson, J. W. Mintmire, *Phys. Rev. B* **1993**, *47*, 5485.
[13] P. N. D'yachkov, D. V. Makaev, *Phys. Rev. B* **2007**, *76*, 195411.
[14] J. B. Conklin, L. E. Johnson, G. W. Pratt, *Phys. Rev.* **1965**, *137*, 1283.
[15] T. L. Loucks, *Phys. Rev.* **1965**, *139*, 1333.
[16] A. H. MacDonald, W. E. Pickettll, D. D. Koelling, *J. Phys. C: Solid State Phys*. **1980**, *13*, 2675.
[17] D. D. Koelling, B. N. Harmon, *J. Phys. C: Solid State Phys*. **1977**, *10*, 3107.
[18] P. N. D'yachkov, D. V. Kirin, *Dokl. Phys. Chem. (Engl. Trans.)*, **1999**, *369*, 326.
[19] P. N. D'yachkov, In Encyclopedia of Nanoscience and Nanotechnology, Vol. *1*; H. S. Nalwa, Ed.; American Scientific: Valencia, CA, **2004**; pp. 191–212.
[20] A. V. Nikolaev, P. N. Dyachkov, *Int. J. Quant. Chem*. **2002**, *89*, 57.
[21] P. N. D'yachkov, *Russ. J. Inorg. Chem*. **2011**, *56*, 2160.
[22] P. N. D'yachkov, O. M. Kepp, In Science and Application of Nanotubes; D. Tomanek, R. J. Enbody, Eds.; Kluwer, Academic/Plenum: New York, **2000**; pp. 77–82.
[23] D. V. Kirin, P. N. D'yachkov, *Dokl. Phys. Chem. (Engl. Trans.)*. **2000**, *373*, 115.
[24] P. N. D'yachkov, D. V. Kirin, in Proceedings of the School and Workshop on Nanotubes and Nanostructures, Vol. *74*; S. Belucci, Ed.; Italian Physical Society: Bologna, Italy, **2001**; pp. 273–280.
[25] V. M. Galitskii, B. M. Karnakov, V. I. Kogan, Zadachi po kvantovoi mekhanike (Problems in Quantum Mechanics); Nauka: Moscow, **1984**.
[26] V. Galitski, B. Karnakov, V. Kogan, V. Galitski, Jr., Exploring Quantum Mechanics: A Collection of 700+ Solved Problems for Students, Lecturers, and Researchers; Oxford University Press: Oxford, **2013**.
[27] G. N. Watson, Treatise on the Theory of Bessel Functions, 2nd ed.; Cambridge University Press: New York, **1966**.
[28] G. A. Korn, T. M. Korn, Mathematical Handbook for Scientists and Engineers; McGraw-Hill: New York, **1961**.
[29] P. N. D'yachkov, H. Hermann, D. V. Kirin, *Appl. Phys. Lett*. **2002**, *81*, 5228.
[30] P. N. D'yachkov, H. Hermann, *J. Appl. Phys*. **2004**, *95*, 399.
[31] M. Damnjanovic, I. Milosevic, Line Groups in Physics. Theory and Applications to Nanotubes and Polymers. Lecture Notes in Physics, Vol. *801*; Springer: Berlin Heidelberg, **2010**.
[32] V. N. Popov, L. Henrard, *Phys. Rev. B* **2004**, *70*, 115407.
[33] P. N. D'yachkov, D. V. Makaev, *Phys. Status Solidi (b)* **2009**, *246*, 140.
[34] D. V. Makaev, P. N. D'yachkov, *Dokl. Phys. Chem*. **2009**, *424*, 10.
[35] P. N. D'yachkov, D. Z. Kutlubaev, D. V. Makaev, *Phys. Rev. B* **2010**, *82*, 035426.
[36] P. Mavropoulos, N. Papanikolaou, In Computational Nanoscience: Do It Yourself!, Vol. 31, NIC Series; J. Grotendorst, S. Blügel, D. Marx, Eds.; John von Neumann Institute for Computing: Jülich, **2006**; pp. 131–158.
[37] P. H. Dederichs, S. Lounis, R. Zeller, In Computational Nanoscience: Do It Yourself!, Vol. 31, NIC Series; J. Grotendorst, S. Blügel, D. Marx, Eds.; John von Neumann Institute for Computing: Jülich, **2006**; pp. 279–298.
[38] J. Korringa, *Physica (Amsterdam)* **1947**, *13*, 392.
[39] W. Kohn, N. Rostoker, *Phys. Rev.* **1954**, *94*, 1111.
[40] V. S. Stepanyuk, A. Szasz, A. A. Katsnelson, A. V. Kozlov, O. V. Farberovich, *Z. Phys. B: Condens. Matter.* **1990**, *81*, 391.
[41] O. V. Farberovich, A. Yaresko, K. Kikoin, V. Fleurov, *Phys. Rev. B* **2008**, *78*, 085206.
[42] P. N. D'yachkov, D. V. Makaev, *Phys. Rev. B* **2006**, *74*, 155442.
[43] D. V. Makaev, P. N. D'yachkov, *JETP Lett*. **2006**, *84*, 335.
[44] R. C. Tatar, S. Rabii, *Phys. Rev. B* **1982**, *25*, 4126.
[45] A. Jensen, J. R. Hauptmann, J. Nygerd, J. Sadowski, P. E. Lindelof, *Nano Lett*. **2004**, *4*, 349.
[46] P. N. D'yachkov, D. V. Makaev, *Phys. Rev. B* **2005**, *71*, 081101(R).
[47] D. V. Makaev, P. N. D'yachkov, *Dokl. Phys. Chem*. **2005**, *402*, 109.
[48] I. A. Bochkov, P. N. D'yachkov, *Russ. J. Inorg. Chem*. **2013**, *58*, 800.
[49] E. P. D'yachkov, L. O. Khoroshavin, I. A. Bochkov, E. M. Kol'tsova, P. N. D'yachkov, *Russ. J. Inorg. Chem*. **2014**, *59*, 682.
[50] P. N. D'yachkov, D. Z. Kutlubaev, *IOP Conference Series: Materials Science and Engineering*, Vol. *38*, **2012**, 012003; International Conference on Functional Materials and Nanotechnologies, Riga, Latvia, 2012.
[51] P. N. D'yachkov, V. A. Zaluev, *J. Phys. Chem. C* **2014**, *118*, 2799.
[52] A. S. Davydov, Quantum Mechanics, 2nd ed.; Pergamon Press: Oxford, New York, **1965**.
[53] L. I. Schiff, Quantum Mechanics; McGraw-Hill: New York, **1949**.
[54] O. M. Kepp, P. N. D'yachkov, *Doklady Akad. Nauk*. **1999**, *3*, 354.
[55] E. V. Larina, V. I. Chmyrev, V. M. Skorikov, P. N. D'yackov, D. V. Makaev, *Inorg. Mater.* **2008**, *44*, 823.
[56] D. V. Kirin, P. N. Dyachkov, *Doklady Phys. Chem*. **2000**, *373*, 115.
[57] D. V. Kirin, P. N. Dyachkov, *Doklady Phys. Chem*. **2001**, *201*, 227.
[58] A. S. Romanov, A. A. Lisenko, P. M. Silenko, P. N. D'yachkov, *JETP Lett*. **2009**, *89*, 558.
[59] I. A. Bochkov, E. P. D'yachkov, P. N. D'yachkov, *Russ. J. Inorg. Chem*. **2014**, *59*, 1448.
[60] P. N. D'yachkov, D. V. Makaev, *J. Phys. Chem. Solids* **2009**, *70*, 180.
[61] A. S. Romanov, D. V. Makaev, P. N. D'yachkov, *JETP Lett*. **2008**, *87*, 50.
[62] A. Y. Golovacheva, P. N. D'yachkov, *JETP Lett*. **2005**, *82*, 737.

Received: 8 June 2015
Revised: 9 July 2015
Accepted: 31 July 2015
Published online 8 September 2015